Synthesis, structure, and corrosion inhibiting properties of RE(III) 3-thiophenecarboxylate complexes

Vidushi Vithana, [a] Zhifang Guo, [a] Glen B. Deacon, [b] Anthony E. Somers [c] and Peter C. Junk [a]*

[a]*College of Science & Engineering, James Cook University, Townsville, 4811, Qld, Australia.*

[b]*School of Chemistry, Monash University, Clayton, 3800, Vic., Australia.*

[c]*Institute for Frontier Materials, Deakin University, Burwood, 3125, Vic., Australia.*

*Corresponding author: peter.junk@jcu.edu.au

Abstract

Two series of Rare Earth (RE) 3-thiophencarboxylate (3TPC) complexes have been synthesized by metathesis reactions between a suitable RE salt and Na(3TPC). Single crystal X-ray diffraction determined that light rare earth metals yield nonacoordinate 1D polymeric complexes $[Ln(3TPC)_3(H_2O)_3]_n$ (**Ln**= La (**1a**), Ce (**1b**), Pr(**1c**), Nd(**1d**), Sm(**1e**), Gd(**1f**)) while the heavier elements have a dimeric structure $[Ln_2(3TPC)_6(H_2O)_4]\cdot H_2O$ (**Ln**= Dy(**2a**), Ho(**2b**), Y(**2c**), Er(**2d**), Lu(**2e**)) with eight coordinated metal centers. Thermogravimetric analysis (TGA) and microanalysis data of all the compounds except for compound **(2e)** are consistent with the composition derived from single-crystal data. However, bulk compound $[Lu_2(3TPC)_6(H_2O)_4]\cdot H_2O$ **(2e)** lost both coordinated and lattice water during the drying process. Based on weight loss measurements, the corrosion inhibitory properties of the synthesized compounds on mild steel show that $[Y_2(3TPC)_6(H_2O)_4]\cdot H_2O$ **(2c)** has the greatest inhibition efficiency (68%). The potentiodynamic polarisation (PP) measurements are generally consistent with immersion test results. However, $[Gd_2(3TPC)_6(H_2O)_4]\cdot H_2O$ **(1e)** exhibited a similar optimum value with an inhibitor efficiency of 70% utilizing this technique. The PP curves show that these compounds act predominantly as anodic inhibitors.

1. Introduction

Corrosion is a widespread and extremely costly issue for engineering materials in diverse industries. To protect metals and alloys from corrosion, a range of approaches are used. Among them, one of the most promising and cost-efficient methods is using corrosion inhibitors.[1–3] Over a century, chromate compounds have been extensively used as corrosion inhibitors for a wide range of metals and alloys.[1,3–6] However, the high toxicity and carcinogenic properties associated with hexavalent chromium have led to a significant reduction in their use.[3,7] Rare earth (RE) salts have shown promise as alternatives to chromates, as they are effective with a relatively low cost and are environmentally friendly substances.[3,8,9]

Corrosion protection by organic corrosion inhibitors is related to the development of protective layers on metals.[10] Among organic systems, compounds containing hetero atoms are considered to have a higher inhibiting performance due to their strong affinity for metallic surfaces.[11–13] A group of CSIRO

researchers developed a rapid screening test to investigate the inhibitive capacity of a series of structurally related compounds on aluminium alloys, and showed that -*para* and -*ortho* thiol substituted carboxylates could strongly inhibit corrosion on AA2024 and AA7075 alloys.[14] Further studies of the inhibitive effect of thiophene derivatives on carbon metal steel suggested that the inhibitive characteristics correlate with the dipole moment of the molecule and the number of adsorption centres present on the molecule. An increase in these features leads to stronger adsorption on the metal surface, hence greater inhibition efficiency.[15–18]

It has been shown that a combination of rare earth metals with organic corrosion inhibitors can form new complexes with improved inhibitory effects. These rare earth carboxylate complexes often suppress both cathodic and anodic reactions by combining the inhibitory properties of the individual components synergistically.[19] Over the past two decades, many rare earth carboxylates have been synthesized[20,21] and a number of them have been tested for corrosion inhibition.[10,19,22–26] Previous studies have found that cerium salicylate[26], lanthanum 4-hydroxycinnamate[7] and yttrium 3-(4'-methylbenzoyl)propionates[27] are excellent inhibitors for mild steel in sodium chloride solutions.

In seeking improved rare earth carboxylate inhibitors, the focus of our current study is on developing new complexes with known and putative organic carboxylic acid inhibitors. The excellent inhibitor properties of thiophene derivatives have led us to investigate the lanthanoid complexation by 3-thiophene carboxylate. Herein we now report the preparation and structural characterization of a range of rare-earth (RE) 3-thiophenecarboxylate (3TPC) complexes (Ln=La, Ce, Pr, Nd, Sm, Gd, Dy, Ho, Y, Er, Lu). The lanthanoid contraction results in the formation of two structural classes. Immersion tests and potentiodynamic polarisation were employed to determine the anti-corrosion properties of these compounds for mild steel, relative to a control.

2. Results and Discussion

2.1 Synthesis and Characterization

The complexes $[Ln(3TPC)_3(H_2O)_3]$ (**Ln**= La, Ce, Pr, Nd, Sm, Gd) and $[Ln_2(3TPC)_6(H_2O)_4]\cdot H_2O$ (**Ln**= Dy, Ho, Y, Er, Lu) were synthesized in moderate yields by metathesis reactions between sodium 3-thiophenecarboxylate and a suitable RE salt (mole ratio 1:3) as shown in Scheme 1.

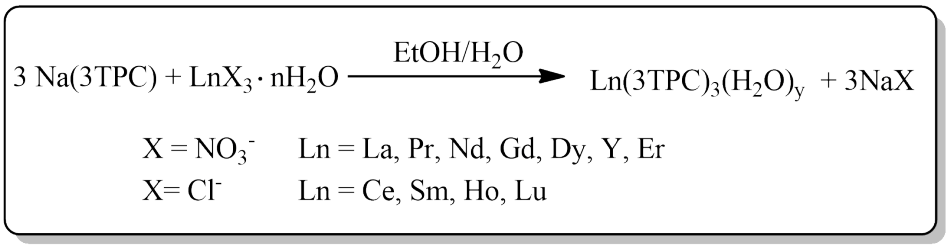

Scheme 1: The synthesis of **Ln** 3-thiophenecarboxylate complexes

In all cases, bulk products were separated as precipitates. Single crystals of the complexes suitable for X-ray crystallography were obtained by slow evaporation of the mother liquor. The compositions of the complexes were derived from X-ray crystallography together with elemental analysis and thermogravimetric analysis (TGA). The characterization of the bulk samples was carried out after drying to constant weight over silica gel. Only the Lu complex **2e** lost water from the single crystal composition under the drying conditions and both coordinated and lattice water was lost. Four

complexes had low % C, a frequent problem with rare earth metal-organic compounds[28–34], but additional % Ln analyses and TGA data leave little doubt as to the bulk composition.

The X-ray powder diffraction patterns of the bulk samples $[Ln(3TPC)_3(H_2O)_3]$ (**Ln**= La**(1a)**, Ce**(1b)**, Pr**(1c)**, Nd**(1d),** Sm**(1d),** Gd**(1e)**) are identical to each other and agree with the simulated pattern of $[Pr(3TPC)_3(H_2O)_3]$ derived from the single-crystal data (Figure S1). Powder XRD analyses of $[Ln_2(3TPC)_6(H_2O)_4]\cdot H_2O$ (**Ln**= Dy**(2a)**, Ho**(2b)**, Y**(2c)**, Er**(2d),** Lu**(2e)**) show similar powder diffractograms and they are almost identical to the generated powder diffractogram for $[Er_2(3TPC)_6(H_2O)_4]\cdot H_2O$ (Figure S2). In the case of **2e,** this similarity obtains despite dehydration**.**

The IR spectra within each isostructural series $[Ln(3TPC)_3(H_2O)_3]$ (**Ln**= La, Ce, Pr, Nd, Sm, Gd) (Figure S3) and $[Ln_2(3TPC)_6(H_2O)_4]\cdot H_2O$ (**Ln**= Dy, Ho, Y, Er, Lu) (Figure S4) are the same, apart from the absence of water absorption for **2e**. Thus, important spectral data are listed for only one compound from each group (**Ln**=Pr**(1c)**; **Ln**= Er**(2d)**). The data of the complexes in series **1** are only slightly different from that of series **2**. This observation suggests comparable binding modes in the compounds with each series. The broad bands at 3200-3550 cm^{-1} are characteristic of the coordinated and lattice water molecules. All the compounds exhibit the strong absorption bands characteristic of asymmetric and symmetric stretching vibrations of the carboxylate groups of the ligand 3TPC at 1530- 1395-cm^{-1}. The relatively small splitting between the asymmetric and symmetric modes are consistent with the bridging and chelating carboxylates exhibited in the structures (below).[35]

Table 1: Selected infrared bands (cm^{-1}) of the RE 3-thiophenecarboxylate complexes

Complex	$\nu(OH)_{water}$	$\nu_{as}(CO_2)$	$\nu_s(CO_2)$	$\Delta\nu$†	$\delta(CO_2)$
$[Pr(3TPC)_3(H_2O)_3]_n$	3381	1525,1493	1395	98	685
$[Er_2(3TPC)_6(H_2O)_4]\cdot H_2O$	3326	1528,1504	1394	110	699

The bulk samples of $[Ln(3TPC)_3(H_2O)_3]_n$ (**Ln**= La, Ce, Pr, Nd, Sm, Gd) and $[Ln_2(3TPC)_6(H_2O)_4]\cdot H_2O$ (**Ln**= Dy, Ho, Y, Er) (discussed above) gave TGA results (Figure S5-6) consistent with the single-crystal compositions, while the TGA data obtained from the bulk sample of $[Lu_2(3TPC)_6(H_2O)_4]\cdot H_2O$ **(2e)** showed significantly different behaviour as the compound had lost all the lattice and coordinated water from the structure derived from the single crystal composition prior to the measurement, and is also evident from elemental analyses. Further defined loss is observed for all the compounds at *ca*. 400-500 °C, plausibly from the decomposition of the anhydrous complexes into $Ln_2(CO_3)_3$ and the diheteroaryl ketone. Such thermal behaviour of metal carboxylates is known.[36] This interpretation is supported by the infrared spectra (Figure S7) of the residues after thermolysis of $[Nd(3TPC)_3(H_2O)_3]_n$ and $[Er_2(3\text{-}TPC)_6(H_2O)_4]\cdot H_2O$ to 500 °C as they corresponded closely to that reported for $[Dy_2(CO_3)_3].4H_2O$.[37] There is evidence of an intermediate formation in the TGA data of **1a-1d,** but not **1e, f.** The weight loss corresponds approximately to formation of $Ln_2(3TPC)_4(CO_3)$ (see Experimental). The instability of this intermediate for **1e, f** perhaps relates to greater stability of the final carbonate species relative to the intermediate as the ionic radius of Ln^{3+} decreases.

2.2 Structural Description

Crystal structures of $[Ln(3TPC)_3(H_2O)_3]_n$ (**Ln**= La, Ce, Pr, Nd, Sm, Gd) and $[Ln_2(3TPC)_6(H_2O)_4]\cdot H_2O$ (**Ln**= Dy, Ho, Y, Er, Lu) were determined. The crystal and refinement data and bond lengths are given in supporting information in Table S1-S5.

The complexes $[Ln(3TPC)_3(H_2O)_3]_n$ (Ln = La, Ce, Pr, Nd, Sm, Gd)

The isostructural series of complexes $[Ln(3TPC)_3(H_2O)_3]_n$ (**Ln**= La **(1a)**, Ce **(1b)**, Pr **(1c)**, Nd **(1d)**, Sm **(1e)**, Gd **(1f)**) form a 1D polymeric chain with nine coordinated rare-earth ions and crystallize in the

monoclinic $P2_1/c$, with a tricapped trigonal prismatic geometry. The representative structure of $[Pr(3TPC)_3(H_2O)_3]_n$ is discussed here, and part of the polymeric structure is shown in Figure 1. The coordination environment of the asymmetric unit comprises two different carboxylate ligand binding modes. There are four chelating oxygen atoms from two κ (O,O') carboxylates (binding through O1,2 and O3,4), one bridging oxygen atom from each of two μ- 1κ(O):2κ(O')- carboxylate (binding through O5,6#2 and three ligated water oxygen atoms (O7, O8, O9). The structure forms a 1D polymeric chain through bridging carboxylate ligand O5#2- C6#1-O6#2 between the 9 coordinated Pr1 and Pr1#1 atoms. The distance between each adjacent Pr metal centre is 6.2763 Å, with Pr1#1-Pr1-Pr1#2 at an angle of 118 .274(13)°. The average Pr-O bond length observed for complex **1c** is 2.526 Å, with the shortest bond Pr1-O5 (2.468 Å) and the longest bond Pr1-O3 (2.577 Å). The former involves a bridging oxygen rather than any of the terminal oxygens. The two chelating rings are quite symmetrical. The ligated water oxygen atoms have angles of 71.056(16)° (O8-Pr1-O9), 67.955(14)° (O9-Pr1-O7), and 135.002(16)° (O7-Pr1-O8) respectively. The two chelating carboxylate ligands have a *trans* disposition C1…Pr1…C11 172.918(3)°. There is hydrogen bonding from one of the bridging oxygen atoms O5 and one water oxygen atom O7#1 attached to the adjacent metal centre. Moreover, a rather unusual H bond forms between O2-H10-C10 resulting in an unusual 7-membered ring. (Fig. 1 and Table S3)

The effect of the ionic radii on the variation in the Ln-O bond length can be examined. (Table S2) A decrease in the average Ln-O bond distance across the RE series from La to Gd [Ln= La 2.565 Å, Ce 2.548 Å, Pr 2.526 Å, Nd 2.510 Å, Sm 2.480 Å, Gd 2.462 Å] is consistent with lanthanoid contraction.[38]

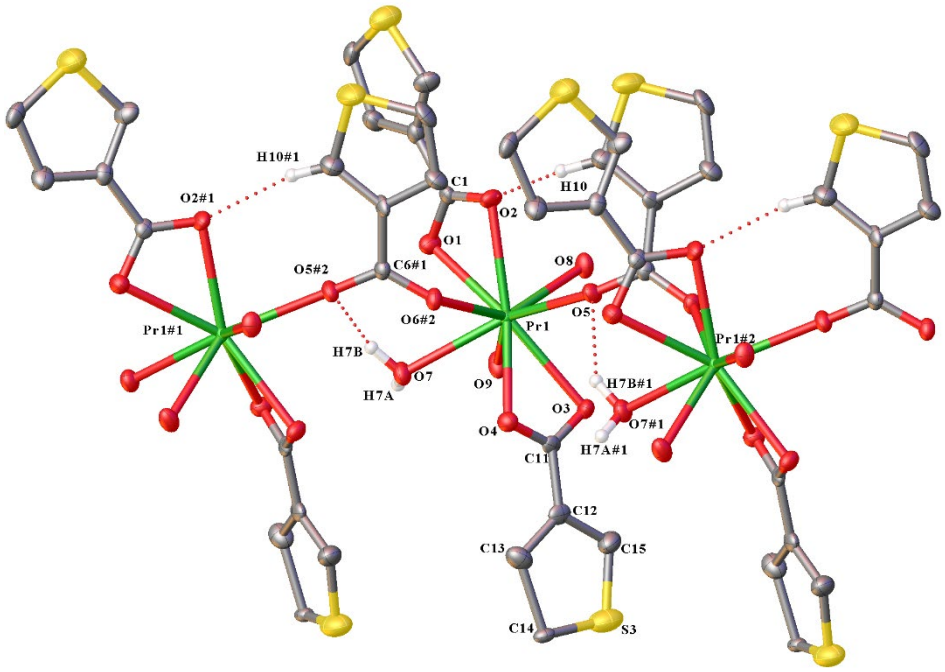

Figure 1. Molecular diagram of $[Pr(3TPC)_3(H_2O)_3]_n$ **(1c)** (representative of La **(1a)**, Ce **(1b)**, Nd **(1d)**, Sm **(1e)**, Gd **(1f)**) The hydrogen atoms except for those forming hydrogen bonds have been omitted for clarity. Selected bond lengths (Å) and angles (°) (Data for **1a-1f** in supplementary information).**1c** Pr1-O1 2.570(5), Pr1-O2 2.531(5), Pr1-O3 2.577(5), Pr1-O4 2.523(5), Pr1-O5 2.468(5), Pr1-O6#1 2.489(5), Pr1-O7 2.538(5), Pr1-O8 2.485(5), Pr1-O9 2.495(5), Pr1#1—Pr1—Pr1#2 118 .274(13), O8-Pr1-O9 71.056(16), O9-Pr1-O7 67.955(14)°, O7-Pr1-O8 135.002(16), C1…Pr1…C11 172.918(3), Symmetry Code: +X,1/2-Y,1/2+Z.

The complexes $[Ln_2(3TPC)_6(H_2O)_4]\cdot H_2O$ (Ln = Dy, Ho, Y, Er, Lu)

The molecular structure of $[Er_2(3TPC)_6(H_2O)_4]\cdot H_2O$ can be found in Figure 2 and is a representative of the isomorphous series of dimeric complexes $[Ln_2(3TPC)_6(H_2O)_4]\cdot H_2O$ (**Ln**= Dy **(2a)**, Ho **(2b)**, Y **(2c)**, Lu **(2e)**) that crystallizes in monoclinic P$2_1/c$ with eight coordinate lanthanoid ions. The stereochemistry of the Ln^{3+} ions can be described as slightly distorted square antiprismatic. The bond lengths of the isostructural series are given in Table S4. Only one half of the centrosymmetric dimer, containing Er1 is unique while Er1#1 is symmetry generated. The carboxylate ligands are coordinated through two different carboxylate binding modes. The complex **2d** contains four κ (O,O') carboxylates binding through the oxygen atoms O1,2 and O3,4 at Er1 and O1#1,2#1 and O3#1,4#1 at Er1#1. The chelating carboxylate ligands show quite symmetric chelation. Two μ- 1κ(O):2κ(O')- carboxylate ligands bridge the two metal centres through O5,6 and O5#1,6#1. Finally, four coordinated water molecules are bound through O7,8 at Er1 and O7#1,8#1 at Er1#1. The Er-O bond length in complex **2d** ranges from 2.229 Å to 2.433 Å with an average of 2.36 Å. Similar to the nine coordinated $Ln(3TPC)_3(H_2O)_3]_n$, the shortest RE-O distance is observed for bridging oxygen. The coordinated water oxygen atoms form a O8-Er1-O7 angle of 85.12(7)° while the two chelating carboxylate ligands form a C1…Er1…C6 angle of 104.735(3)°. This contrasts their *trans* disposition in **1c**. The bridging oxygen atoms form an angle of 114.374(4)° between themselves through O5-Er1-O6#1. There is hydrogen bonding involving two of the κ (O,O') carboxylate oxygen atoms O4, 4#1, two of the ligated water oxygen atoms O7#1,O7 and the lattice water oxygen atom O9 in the dimeric structure. (Table S5)

In accord with the lanthanoid contraction, a decrease in the average Ln-O bond lengths across the series from Dy to Lu (Ln= Dy 2.390, Ho 2.374, Y 2.367, Er 2.360, Lu 2.328) is observed.[38]

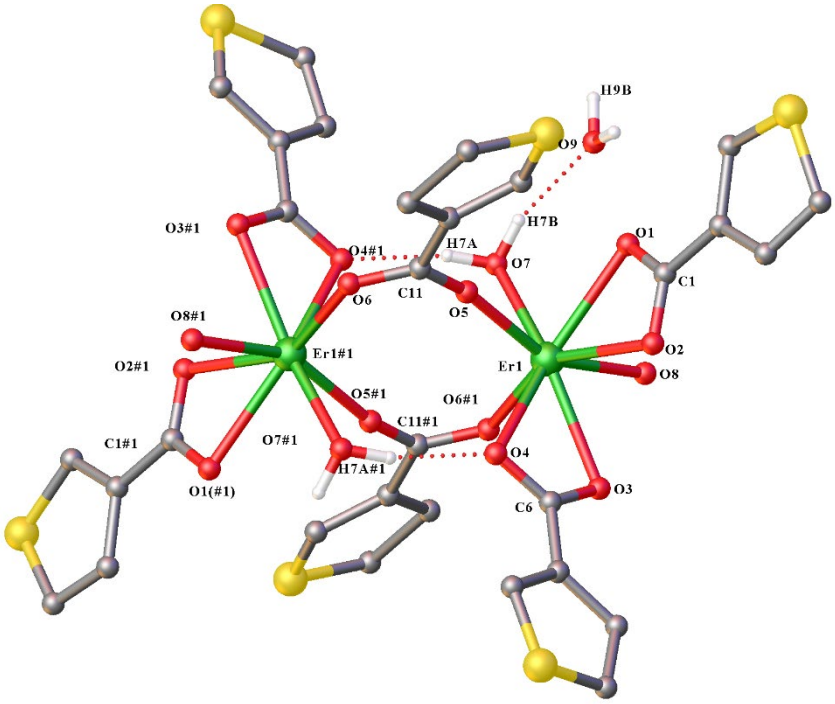

Figure 2. Molecular diagram of $[Er_2(3TPC)_6(H_2O)_4]\cdot H_2O$ **(2d)** (representative of Dy **(2a)**, Ho **(2b)**, Y **(2c)**, Lu **(2e)**) The hydrogen atoms except for those having hydrogen bonds have been omitted for clarity. Selected bond lengths (Å) (Data for **2a-2e** in supplementary information). **2d** Er1-O1 2.426(2), Er1-O2 2.398(2), Er1-O3 2.433(2), Er1-O4 2.394(2), Er1-O5 2.229(2), Er1-O6#1 2.283(2), Er1-O7 2.385(2), Er1-O8 2.330(2) O8-Er1-H7A 85.124(6), C1…Er1…C6 104.735(3), O5-Er1-O6#1 114.374(4). Symmetry Code: 2-X,1-Y,1-Z.

2.3 Corrosion Inhibition

2.3.1 Immersion Tests

Table 2 provides a summary of the results obtained from weight loss measurements for steel coupons over seven days in 0.01M NaCl solutions in the presence of $RE(3TPC)_3$. At the end of the test period, visual inspections (Figure S8) of all the coupons indicated dullness and signs of pitting. However, when considering the general uniformity, the coupons placed in inhibitor solutions were significantly less affected compared to the control coupons. The weight loss of the coupons during the immersion test period is considered the primary measure of corrosion. Thus, the corrosion rates of the inhibitor solutions were calculated by using the equation described in eq1:

$$\text{Corrosion rate (R)} = \frac{KW}{ATD} \quad (1)$$

Where:
K= A constant; W = Weight loss (g); A = Coupon area (cm^2) T= Time of exposure (168 h);
D = Density of the test metal

Then using these data, the percentage corrosion inhibition (η) of each compound was calculated. (Eq 2):

$$\eta = \frac{R(Control) - R\,(inhibitor)}{R(Control)} \times 100 \quad (2)$$

Consistent with visual inspections, weight loss measurements also indicated that $[La(3TPC)_3(H_2O)_3]_n$ **(1a)** has the lowest inhibition efficiency with an η = 36.5% and $[Y_2(3TPC)_6(H_2O)_4]\cdot H_2O$ **(2c)** resulted in the best performance with nearly 68% of effectiveness at the concentration used in the experiment (500 ppm). The inhibitive properties of the compounds correlate to some extent with the decreasing atomic radius of rare earth metals, but Gd and Y are positive outliers and Nd and Lu negative ones. The light rare earth (La-Nd) complexes were less effective than the heavier derivatives with Pr the best performer of the former group. In this context, it is interesting that the anti-corrosion performance of cerium diphenyl phosphate is enhanced by Pr.[39] The overall trend is dissimilar to behaviour of salicylate[26] and 4-hydroxycinnamate[7] complexes where Ce and La complexes respectively perform best. With heavier lanthanoids there is improved protection from Sm to Gd and then near similar behavior from Gd-Er with a decline to Lu. However, Y with a similar ionic radius to Er performs best, reminiscent of the superiority of the yttrium complex in the 3-(4'-methylbenzoyl)propanoate series.[27] This reinforces increasing evidence that the influence of the rare earth is ligand dependent. The low solubility of the complexes has deterred pursuing attempts at higher concentrations.

Table 2: Corrosion rates ($\mu gm^{-2}s^{-1}$, mmy^{-1}) and percentage inhibition (η) for mild steel coupons immersed in specific solutions for seven days

Solution	Concentration		Solubilities[a]		Avg Weight Loss (mg)	Corrosion Rate ($\mu gm^{-2}s^{-1}$)	Corrosion Rate (mmy^{-1})	Percentage Inhibition (η)
	ppm	M	In H_2O	In NaCl (0.01M)				
Control - NaCl	580	0.01			16.5	30.5	0.1221	0
$[La(3TPC)_3(H_2O)_3]_n$	500	8.71×10^{-4}	900	580	10.4	19.36	0.0775	36.5
$[Ce(3TPC)_3(H_2O)_3]_n$	500	8.69×10^{-4}	900	590	9.95	18.8	0.0753	38.4
$[Pr(3TPC)_3(H_2O)_3]_n$	500	8.67×10^{-4}	900	590	8.99	16.28	0.0652	46.6

$[Nd(3TPC)_3(H_2O)_3]_n$	500	8.63×10^{-4}	950	590	9.75	18.91	0.0757	38.0
$[Sm(3TPC)_3(H_2O)_3]_n$	500	8.53×10^{-4}	850	550	7.55	14.87	0.0595	51.2
$[Gd(3TPC)_3(H_2O)_3]_n$	500	8.44×10^{-4}	790	520	6.0	11.87	0.0475	61.1
$[Dy_2(3TPC)_6(H_2O)_4].\ H_2O$	500	4.25×10^{-4}	920	520	6.77	12.62	0.0506	58.6
$[Ho_2(3TPC)_6(H_2O)_4].\ H_2O$	500	4.23×10^{-4}	870	530	6.0	12.01	0.0481	60.6
$[Y_2(3TPC)_6(H_2O)_4].\ H_2O$	500	4.85×10^{-4}	600	500	5.3	9.65	0.0386	68.4
$[Er_2(3TPC)_6(H_2O)_4].\ H_2O$	500	4.21×10^{-4}	700	540	6.25	11.58	0.0464	62.0
$[Lu_2(3TPC)_6]$	500	4.49×10^{-4}	900	550	7.3	14.13	0.0565	53.7

[a] Solubilities of the compounds in 0.01 M NaCl solution were lower than that in distilled water. Therefore, the immersion tests were done with the compounds at 500 ppm concentration.

2.3.2 Potentiodynamic polarisation

The results of the potentiodynamic polarisation experiments are shown in Table 3. $[Gd_2(3TPC)_6(H_2O)_4]\cdot H_2O$ **(1e)** and $[Y_2(3TPC)_6(H_2O)_4]\cdot H_2O$ **(2c)** showed the lowest i_{corr}, at 0.953 and 0.981 $\mu A/cm^2$ respectively. With the compounds present in the solution there is a shift in E_{corr} to more positive values as compared to the control, indicative of anodic inhibition dominating the reduction in i_{corr}. Representative PP scans in Figure S9 show the marked reduction in the anodic arm when the compounds are present, with some reduction in the cathodic kinetics. Such a response is typical of these types of compounds.[5] However, the performance of the yttrium compound was somewhat inferior to that of yttrium 3-(4'-methylbenzoyl)propanoate.[40]

Table 3: Summary of corrosion parameters obtained from potentiodynamic polarisation tests in control and inhibited solutions after 24 h immersion.

Solution	i_{corr} ($\mu A/cm^2$)	Std. Dev.	E_{corr} (mV)	Std. Dev.	Percentage Inhibition
Control - NaCl	2.875	0.108	-638	4	-
$[Gd(3TPC)_3(H_2O)_3]_n$	0.953	0.135	-515	5	70
$[Y_2(3TPC)_6(H_2O)_4].\ H_2O$	0.981	0.121	-530	9	68
$[Er_2(3TPC)_6(H_2O)_4].\ H_2O$	1.414	0.263	-578	6	38

3. Conclusion

A series of RE 3-thiophenecarboxylate complexes have been successfully synthesized and characterized. All the compounds crystallized in one of the two structural groups based on single-crystal X-ray crystallography and on powder diffraction with similar IR spectra and TGA behaviour within each class. Type 1 structures, $[Ln(3TPC)_3(H_2O)_3]_n$ (**Ln**= La, Ce, Pr, Nd, Sm, Gd), are one dimensional polymers in which the coordination number of the Ln atom is nine. By contrast, Type 2 compounds form dimeric structures, $[Ln_2(3TPC)_6(H_2O)_4]\cdot H_2O$ (**Ln**= Dy, Ho, Y, Er, Lu), with a lanthanoid coordination number of eight. The lanthanoid contraction is reflected in a reduction of Ln-O bond lengths as well as the decrease in coordination number.

Weight loss measurements indicate that $[Y_2(3TPC)_6(H_2O)_4]\cdot H_2O$ **(2c)** has the best corrosion inhibition performance for mild steel in aqueous NaCl solution, while $[La(3TPC)_3(H_2O)_3]_n$ **(1a)** is the least effective. Potentiodynamic polarisation confirmed the superior performance of $[Y_2(3TPC)_6(H_2O)_4]\cdot H_2O$

(2c) but also gave a similar result for $[Gd_2(3TPC)_6(H_2O)_4]\cdot H_2O$ **(1e)**. The compounds act predominantly as anodic inhibitors. A comparison of Y complex data suggests introduction of a thiophene moiety into a carboxylate is not quite as effective as a 3-(4'-methylbenzoyl) group.[40]

4. Experimental Section

4.1 General Method and Reagents

All commercially available solvents and chemicals were purchased from Sigma-Aldrich or BDH and used without further purification. Elemental analysis (C, H) was performed by either the Elemental Analysis Service Team, Science Centre, London Metropolitan University, England or the Chemical Analysis Facility, Department of Molecular Sciences, Macquarie University, NSW. Metal analysis was conducted by complexometric titration with 0.01 M EDTA using hexamethylenetetramine as a buffer and xylenol orange indicator. IR spectra were recorded on Nicolet™ iS™ 5 FTIR Spectrometer as in the range of 4000-500 cm^{-1}. Thermogravimetric analysis (TGA) was performed on TA instrument SDT 650 using the standard 90 µl alumina metal pans in an N_2 atmosphere (50 $mlmin^{-1}$) from room temperature up to 750 ℃ (with a ramp of 10 ℃min^{-1}). Powder diffraction patterns (PXRD) were measured at room temperature using a Bruker D2 PHASER diffractometer in the range of 2-60° with a 0.2° divergence slit and at 0.02° increments. The simulated powder patterns were generated from single-crystal X-ray diffraction data using the Mercury program provided by Cambridge Crystallographic Data Centre.[41] Melting points were determined in glass capillaries and are uncalibrated.

4.2 X-ray Crystallography

Single crystals were mounted on glass fibres or loops using viscous hydrocarbon oil on the respective diffractometer. For the complexes **2a, 2d, 2e** data were collected using a Rigaku SynergyS diffractometer. The SynergyS operated using microsource Mo-Kα radiation (λ = 0.71073 Å) at 123 K. The complexes **1b, 1c, 2b** were measured on Oxford Diffraction Gemini Ultra dual source (Mo and Cu) CCD diffractometer collected at 123 K using either Mo X-ray source (λ = 0.71073 Å) or Cu source (λ = 1.54184 Å). Data processing was conducted using CrysAlisPro.55 software suite.[42] The rest of the compounds (**1a, 1d, 1e, 1f, 2c**) were collected on the MX1 beamline at the Australian Synchrotron. The data integration was processed with Blue-ice[43] and XDS[44] software programs. Structures were solved by SHELXT and refined by full-umatrix least-squares methods against F2 using SHELX2018,[45] utilizing the Olex2 [46] graphical user interface. All hydrogen atoms were placed in calculated positions using the riding model. Crystal data and refinement details are shown in Table S1. CCDC 2183938-2183943 for **1a-1f** and 2183944-2183948 for **2a-2e**, contain the supplementary crystallographic data for this paper. These data can be obtained free of charge from The Cambridge Crystallographic Data Centre.

4.3 Synthesis of 3-thiophenecarboxylate(3TPC)- RE aqua complexes

General Synthetic Method: 3-thiophenecarboxylic acid was dissolved in 95% ethanol (15ml) and treated with an equimolar amount of NaOH in distilled water (10 ml). The solution was stirred for 1 h and the pH was adjusted to 7-8. Three molar equivalent of the sodium 3-thiophenecarboxylate was slowly added to one equivalent of the lanthanoid salt solution and stirred for 2 hours while maintaining the pH at 5. The resultant precipitate was collected and washed with distilled water followed by ethanol and air-dried for 2-3 days. The mother liquor was allowed to slowly evaporate at room temperature and XRD-suitable single crystals were separated from it.

$[La(3TPC)_3(H_2O)_3]_n$ (1a)

$[La(3TPC)_3(H_2O)_3]_n$ White colour Powder Yield: 86%, m.p. >300 ℃. Elemental analysis for $C_{15}H_{15}LaO_9S_3$ (MW: 574.37 $gmol^{-1}$): Calculated (%) C 31.37; H 2.63; La 24.18. Found (%) C 31.56; H 2.50; La 23.39. IR (cm^{-1}): 3376m, 3113m, 1607w, 1556m, 1524s, 1494s, 1441s, 1397s, 1351s, 1123w, 1078w, 935w, 871w, 835m, 776s, 755s, 626m, 685m, 578s, 520s, 411s; TGA weight loss (50-110 ℃); 9.09% (Calc. for loss of 3×H_2O= 9.40%); weight loss (340-460 ℃); 15.4% (Calc. for formation of $La_2(CO_3)(O_2CR)_4$= 16.9%); weight loss (340-540 ℃); 38.0% (Calc. for formation of $La_2(CO_3)_3$= 39.8%)

$[Ce(3TPC)_3(H_2O)_3]_n$ (1b)

$[Ce(3TPC)_3(H_2O)_3]_n$ White colour Powder Yield: 73%, m.p. >300 ℃. Elemental analysis for $C_{15}H_{15}CeO_9S_3$ (MW: 575.58 $gmol^{-1}$): Calculated (%) C 31.30; H 2.63; Ce 24.34. Found (%) C 31.46; H 2.48; Ce 24.26. IR (cm^{-1}): 3380m, 3113m, 1608w, 1554m, 1522s, 1492s, 1440s, 1396s, 1348s, 1123w, 1077w, 935w, 871w, 835m, 776s, 754s, 626m, 685s, 578s, 521s, 408s; TGA weight loss (50-110 ℃); 9.02% (Calc. for loss of 3×H_2O= 9.38%); %); weight loss (330-450 ℃); 15.7% (Calc. for formation of $Ce_2(CO_3)(O_2CR)_4$= 16.9%); weight loss (330-560 ℃); 37.5% (Calc. for formation of $Ce_2(CO_3)_3$= 39.9%)

$[Pr(3TPC)_3(H_2O)_3]_n$ (1c)

$[Pr(3TPC)_3(H_2O)_3]_n$ pale green colour Powder Yield: 76%, m.p. >300 ℃. Elemental analysis for $C_{15}H_{15}O_9PrS_3$ (MW: 576.38 $gmol^{-1}$): Calculated (%) C 31.26; H 2.62; Pr 24.45. Found (%) C 31.42; H 2.54; Pr 24.11. IR (cm^{-1}): 3381m, 3112m, 1609w, 1556m, 1525s, 1493s, 1441s, 1395s, 1351s, 1123w, 1078w, 935w, 871w, 836m, 777s, 754s, 685s, 627m, 579s, 520s, 411s. TGA weight loss (50-110 ℃); 9.43% (Calc. for loss of 3×H_2O= 9.37%); %); weight loss (340-450 ℃); 16.4% (Calc. for formation of $Pr_2(CO_3)(O_2CR)_4$= 16.9%); weight loss (340-560 ℃); 39.2% (Calc. for formation of $Pr_2(CO_3)_3$= 40.1%)

$[Nd(3TPC)_3(H_2O)_3]_n$ (1d)

$[Nd(3TPC)_3(H_2O)_3]_n$ purple colour Powder Yield: 76%, m.p. >300 ℃. Elemental analysis for $C_{15}H_{15}NdO_9S_3$ (MW: 579.71 $gmol^{-1}$): Calculated (%) C 31.08; H 2.61; Nd 24.88. Found (%) C 31.28; H 2.49; Nd 24.62. IR (cm^{-1}): 3379m, 3114m, 1611w, 1557m, 1522s, 1492s, 1441s, 1395s, 1351m, 1123w, 1078w, 871w, 836m, 777s, 754s, 626m, 685s, 579s, 521s, 408s. TGA weight loss (50-110 ℃); 9.74% (Calc. for loss of 3×H_2O= 9.31%); weight loss (340-450 ℃); 17.2% (Calc. for formation of $Nd_2(CO_3)(O_2CR)_4$= 16.8%); weight loss (340-560 ℃); 41.6% (Calc. for formation of $Nd_2(CO_3)_3$= 40.4%)

$[Sm(3TPC)_3(H_2O)_3]_n$ (1e)

$[Sm(3TPC)_3(H_2O)_3]_n$ white colour Powder Yield: 54%, m.p. >300 ℃. Elemental analysis for $C_{15}H_{15}O_9S_3Sm$ (MW: 585.83 $gmol^{-1}$): Calculated (%) C 30.75; H 2.58; Sm 25.67. Found (%) C 29.49; H 2.23; Sm 25.95. IR (cm^{-1}): 3373m, 3116m, 1612w, 1559m, 1522s, 1491s, 1438s, 1395s, 1351s, 1123w, 1078w, 935w, 872w, 836m, 754s, 627m, 684s, 579s, 519s, 414s. TGA weight loss (55-120 ℃); 9.07% (Calc. for loss of 3×H_2O= 9.17%); weight loss (370-540 ℃); 37.0% (Calc. for formation of $Sm_2(CO_3)_3$= 40.8%)

$[Gd(3TPC)_3(H_2O)_3]_n$ (1f)

$[Gd(3TPC)_3(H_2O)_3]_n$ white colour Powder Yield: 63%, m.p. >300 ℃. Elemental analysis for $C_{15}H_{15}GdO_9S_3$ (MW: 592.72 $gmol^{-1}$): Calculated C 30.40; H 2.55; Gd 26.53. Found (%) C 29.22; H 2.16; Gd 26.96. IR (cm^{-1}): 3382m, 3118m, 1566m, 1529s, 1495s, 1431s, 1396m, 1354s, 1124w, 1079w, 873m, 838m, 784m, 755s, 685s, 627m, 580m, 522s, 414s. TGA weight loss (55-115 ℃); 9.0% (Calc. for loss of 3×H_2O= 9.11 %); weight loss (370-550 ℃); 38.5% (Calc. for formation of $Gd_2(CO_3)_3$= 41.7%)

$[Dy_2(3TPC)_6(H_2O)_4]\cdot H_2O$ (2a)

$[Dy_2(3\text{-}TPC)_6(H_2O)_4]\cdot H_2O$ white colour powder Yield: 69%, m.p. >300℃. Elemental analysis for $C_{30}H_{28}Dy_2O_{17}S_6$ (MW: 1177.92 $gmol^{-1}$): Calculated (%) C 30.59; H 2.40; Dy 27.59. Found (%) C 29.37; H 2.12; Dy 27.19. IR (cm^{-1}): 3254 w, 3109w, 1557m, 1527s, 1503s, 1434s, 1346s, 1209w, 1123w, 1073w, 940w, 875w, 837s, 780s, 755s, 699m, 628m, 526m, 423s. TGA weight loss (40-95 ℃); 7.76 % (Calc. for loss of $5\times H_2O$= 7.64%); weight loss (380-570 ℃); 38.5% (Calc. for formation of $Dy_2(CO_3)_3$= 42.9%)

$[Ho_2(3\text{-}TPC)_6(H_2O)_4]\cdot H_2O$ (2b)

$[Ho_2(3\text{-}TPC)_6(H_2O)_4]\cdot H_2O$ yellow colour powder Yield: 85%, m.p. >300℃. Elemental analysis for $C_{30}H_{28}Ho_2O_{17}S_6$ (MW: 1182.78 $gmol^{-1}$): Calculated (%) C 30.46; H 2.39; Ho 27.89. Found (%) C 29.97; H 2.25; Ho 28.84. IR (cm^{-1}): 3292w, 3111w, 1566m, 1528s, 1503s, 1428s, 1348s, 1123w, 1073w, 940w, 875w, 837m, 781m, 754s, 699m, 627m, 526m, 420s. TGA weight loss (40-95 ℃); 7.19 % (Calc. for loss of $5\times H_2O$= 7.61%); weight loss (395-570 ℃); 36.1% (Calc. for formation of $Ho_2(CO_3)_3$= 43.1%)

$[Y_2(3\text{-}TPC)_6(H_2O)_4]\cdot H_2O$ (2c)

$[Y_2(3\text{-}TPC)_6(H_2O)_4]\cdot H_2O$ white colour powder Yield: 69%, m.p. >300℃. Elemental analysis for $C_{30}H_{28}O_{17}S_6Y_2$ (MW: 1030.73 $gmol^{-1}$): Calculated (%) C 34.96; H 2.74; Y 17.25. Found (%) C 33.38; H 2.53; Y 17.55. IR (cm^{-1}): 3341w, 3106w, 1567m, 1529s, 1504s, 1434s, 1402s, 1349s, 1209w, 1123w, 1073w, 940w, 875 w, 838m, 782m, 754s, 698s, 627m, 550m, 525m, 422s. TGA weight loss (40-95 ℃); 8.29% (Calc. for loss of $5\times H_2O$= 8.73%); weight loss (400-570 ℃); 38.4% (Calc. for formation of $Y_2(CO_3)_3$= 34.7%)

$[Er_2(3\text{-}TPC)_6(H_2O)_4]\cdot H_2O$ (2d)

$[Er_2(3\text{-}TPC)_6(H_2O)_4]\cdot H_2O$ pink colour powder Yield: 72%, m.p. >300℃. Elemental analysis for $C_{30}H_{28}Er_2O_{17}S_6$ (MW: 1187.44 $gmol^{-1}$): Calculated (%) C 30.34; H 2.38; Er 28.17. Found (%) C 30.32; H 2.36; Er 28.5. IR (cm^{-1}): 3326w, 3106w, 1568m, 1528s, 1504s, 1435s, 1394s, 1348s, 1123w, 1073w, 941w, 875w, 837m, 782m, 754s, 699m, 627m, 525m, 423s. TGA weight loss (40-95 ℃); 7.36% (Calc. for loss of $5\times H_2O$= 7.58%); weight loss (380-600 ℃); 43.7% (Calc. for formation of $Er_2(CO_3)_3$= 43.3%)

$[Lu_2(3\text{-}TPC)_6(H_2O)_4]\ H_2O$ (2e)

$[Lu_2(3\text{-}TPC)_6(H_2O)_4]\ H_2O$ white colour powder Yield: 84%, m.p. >300℃. Elemental analysis calculated for $C_{30}H_{28}Lu_2O_{17}S_6$ (MW: 1202.86 $gmol^{-1}$) Calculated (%) C 30.16; H 1.69; Lu 29.29: $C_{30}H_{18}Lu_2O_{12}S_6$ (MW: 1112.78 $gmol^{-1}$, loss of 5 H_2O) Calculated (%) C 32.35; H 1.62; Lu 31.45. Found (%) C 32.04; H 1.56; Lu 32.07. IR (cm^{-1}): 3103w, 1610w, 1515s, 1428s, 1396s, 1339s, 1208w, 1125w, 1071w, 941w, 873w, 834m, 754s, 699m, 626m, 529w, 430s. TGA weight loss (340-600 ℃); 43.8% (Calc. for formation of $Lu_2(CO_3)_3$= 44.1%)

4.4 Corrosion Testing

Weight loss experiments were conducted according to the standard method ASTM G31-72[47] to assess the general corrosion and inhibition behaviour of synthesized compounds. Mild steel AS 1020 coupons were cut to approximately 20×20×1.5 mm and each of them was abraded progressively with sanding sheets of 80, 120, 240, 360, 800, 1200 and 2000 grits. Then the specimens were firstly rinsed with distilled water secondly with ethanol and dried under N_2 gas. A series of immersion tests were conducted immediately after polishing the coupons, up to 168h (7 days) in 0.01 M NaCl solutions with and without 500 ppm of the inhibitor compounds. Upon the completion of the test, the coupons were rinsed with distilled water. The corrosion product stuck to the substrate was firstly removed by

sonicating in clean water followed by using finest sanding papers with minimum force to avoid the removal of sound material. Finally, the coupons were washed with ethanol and dried with N_2 gas.

The same solutions were used for the compounds containing REs Y, Gd and Er to conduct Potentiodynamic Polarisation (PP) experiments, as these compounds showed the best performance in weight loss experiments. The tests were conducted on a Bio-Logic VMP3 multi-channel potentiostat in a three-electrode cell with an AS1020 steel rod as the working electrode surface, a titanium mesh counter electrode and a Ag/AgCl reference electrode, which was positioned very close to the working electrode surface. The steel rod was encased in epoxy, with a 10mm diameter exposed and polished to a 1200 grit finish. For each PP experiment 100mL of the test solution was used, with the solution quiescent and open to air. The Open Circuit Voltage (OCV) was monitored for 24 hours followed by the PP scan at a rate of 0.167mV/s over a scan range of 150mV below to 250mV above OCV. Corrosion current density (i_{corr}) and corrosion potential (E_{corr}) were extracted from the PP curves using Tafel extrapolation in EC Lab software V11.27. The curves were approximately linear over a range of 10-25 mV either side of E_{corr} and so the Tafel extrapolations were made over the data in this range. This range was chosen as it is in the activation region for this solution type. The point where the linear section of the anodic and cathodic sections of the PP curves intersected the value for E_{corr} was used to determine i_{corr}.

Conflicts of Interest

There are no conflicts of interest to declare. PCJ is an Associate Editor at New Journal of Chemistry.

Acknowledgement

PCJ and GBD gratefully acknowledge the ARC for funding (DP200100568). Parts of this research were undertaken on the MX1 beamline at the Australian Synchrotron, part of ANSTO.[48] The authors also acknowledge crystallographic assistance from Professor P.V. Bernhardt.

References

1 A. L. Chong, J. I. Mardel, D. R. MacFarlane, M. Forsyth and A. E. Somers, *ACS Sustain. Chem. Eng.*, 2016, **4**, 1746–1755.

2 M. Ghorbani, J. Soto Puelles, M. Forsyth, R. A. Catubig, L. Ackland, L. Machuca, H. Terryn and A. E. Somers, *J. Phys. Chem.*, 2020, **11**, 9886–9892.

3 J. Sinko, *Prog. Org. Coat.*, 2001, **42**, 267–282.

4 Y. Peng, A. E. Hughes, G. B. Deacon, P. C. Junk, B. R. W. Hinton, M. Forsyth, J. I. Mardel and A. E. Somers, *Corros. Sci.*, 2018, **145**, 199–211.

5 F. Blin, S. G. Leary, K. Wilson, G. B. Deacon, P. C. Junk and M. Forsyth, *J. Appl. Electrochem.,* 2004, **34**, 591–599.

6 M. Forsyth, T. Markley, D. Ho, G. B. Deacon, P. Junk, B. Hinton and A. Hughes, *Corrosion*, 2008, **64**, 191–197.

7 F. Blin, S. G. Leary, G. B. Deacon, P. C. Junk and M. Forsyth, *Corros. Sci.*, 2006, **48**, 404–419.

8 B. Hinton, Corrosion prevention and control, in *Handbook on the Physics and Chemistry of Rare Earths*, ed. K.A. Gschneidner, Jr. and L. Eyring, Elsevier Science B.V., 1995, vol. 21, pp. 29–92.

9 B. R. W. Hinton, *J. Alloys Compd.*, 1992, **180**, 15–25.

10 T. Markley, F. Blin, M. Forsyth and B. Hinton, Multifunctional rare earth organic corrosion inhibitors in *Rare Earth-Based Corrosion Inhibitors*, ed. M. Forsyth and B. Hinton, Woodhead Publishing, Cambridge, 2014, Ch. 4.

11 D. A. Winkler, M. Breedon, A. E. Hughes, F. R. Burden, A. S. Barnard, T. G. Harvey and I. Cole, *Green Chem.*, 2014, **16**, 3349–3357.

12 D. Daoud, T. Douadi, H. Hamani, S. Chafaa and M. Al-Noaimi, *Corros. Sci.*, 2015, **94**, 21–37.

13 C. Verma, E. E. Ebenso and M. A. Quraishi, Ionic Liquids as Green Corrosion Inhibitors for Industrial Metals and Alloys in *Green Chemistry, ed Hosam El-Din M. Saleh and Martin Koller*, IntechOpen, London, 2018, Ch. 6.

14 T. G. Harvey, S. G. Hardin, A. E. Hughes, T. H. Muster, P. A. White, T. A. Markley, P. A. Corrigan, J. Mardel, S. J. Garcia, J. M. C. Mol and A. M. Glenn, *Corros. Sci.*, 2011, **53**, 2184–2190.

15 A. Galal, N. F. Atta and M. H. S. Al-Hassan, *Mater. Chem. Phys.*, 2005, **89**, 38–48.

16 Z. Szklarska-Smialowska and M. Kaminski, *Corros. Sci.*, 1973, **13**, 10.

17 A. S. Fouda, *Monatsh. Chem.*, 1986, **117**, 159–165.

18 A. S. Fouda, A. A. Ibrahim and W. T. El-Behairy, *Der Pharma Chem.*, 2014, **6**, 144–157.

19 M. Forsyth, K. Wilson, T. Behrsing, C. Forsyth, G. B. Deacon and A. Phanasgoankar, *Corrosion*, 2002, **8,** 953-960.

20 A. E. Somers, Y. Peng, A. L. Chong, M. Forsyth, D. R. MacFarlane, G. B. Deacon, A. E. Hughes, B. R. W. Hinton, J. I. Mardel and P. C. Junk, *Corros. Eng. Sci. Technol.*, 2020, **55**, 311–321.

21 A. E. Somers, G. B. Deacon, B. R. W. Hinton, D. R. Macfarlane, P. C. Junk, M. Y. J. Tan and M. Forsyth, *J. Indian Inst. Sci.*, 2016, **96**, 285–292.

22 T. Behrsing, G. B. Deacon and P. C. Junk, The chemistry of rare earth metals, compounds, and corrosion inhibitors in *Rare Earth-Based Corrosion Inhibitors*, ed. M. Forsyth and B. Hinton, Woodhead Publishing, Cambridge, 2014, Ch. 1.

23 R. Janicki, A. Mondry and P. Starynowicz, *Coord. Chem. Rev.*, 2017, **340**, 98–133.

24 J. de Damborenea, A. Conde and M. A. Arenas, Corrosion Inhibition with Rare Earth Metal Compounds in Aqueous Solution, in *Rare Earth-Based Corrosion Inhibitors*, ed. M. Forsyth and B. Hinton, Woodhead Publishing, Cambridge, 2014, Ch.3.

25 A. E. Hughes, T. G. Harvey, N. Birbilis, A. Kumar and R. G. Buchheit, Coatings for corrosion prevention based on rare earths in *Rare Earth-Based Corrosion Inhibitors*, ed. M. Forsyth and B. Hinton, Woodhead Publishing, Cambridge, 2014, Ch. 7.

26 M. Forsyth, M. Seter, B. Hinton, G. Deacon and P. Junk, *Aust. J. Chem.*, 2011, **64**, 812–819.

27 Y. Peng, A. E. Hughes, G. B. Deacon, P. C. Junk, B. R. W. Hinton, M. Forsyth, J. I. Mardel and A. E. Somers, *Corros. Sci.*, 2018, **145**, 199–211.

28 M. Salehisaki, N. E. Rad, G. B. Deacon, J. Wang, Z. Guo and P. C. Junk, *Inorg. Chim. Acta.*, 2022, **539**, 120997.

29 G. J. Moxey, A. J. Blake, W. Lewis and D. L. Kays, *Eur. J. Inorg. Chem.*, 2015, **2015**, 5892–5902.

30 R. P. Kelly, T. D. M. Bell, R. P. Cox, D. P. Daniels, G. B. Deacon, F. Jaroschik, P. C. Junk, X. F. le Goff, G. Lemercier, A. Martinez, J. Wang and D. Werner, *Organometallics*, 2015, **34**, 5624–5636.

31 H. Sitzmann, T. Dezember, O. Schmitt, F. Weber, G. Wolmershäuser and M. Ruck, *Z. Anorg. Allg. Chem.*, 2000, **626**, 2241–2244.

32 L. H. J. Lajunen and G. R. Choppin, *Rev. Anal. Chem.*, 1989, **9**, 91–130.

33 D. P. Daniels, G. B. Deacon, D. Harakat, F. Jaroschik and P. C. Junk, *J. Chem. Soc., Dalton Trans.*, 2012, **41**, 267–277.

34 L. Hirneise, C. Maichle-Mössmer and R. Anwander, *Inorg. Chem.*, 2021, **60**, 18211–18224.

35 G. B. Deacon and R. J. Phillips, *Coord. Chem. Rev.*, 1980, **33**, 227–250.

36 (a) G. B. Deacon, S. J. Faulks and G. N. Pain, *Adv. Organomet. Chem.*, 1986, **25**, 237–276; (b) G. B. Deacon, *Organometal. Chem. Rev. A*, 1970, **5**, 355.

37 B. Vallina, J. D. Rodriguez-Blanco, A. P. Brown, J. A. Blanco and L. G. Benning, *J. Nanopart. Res.,* 2013, **15**, 1438.

38 R. D. Shannon, *Acta Crystallogr. A*, 1976, **32**, 751–767.

39 T.A. Markley, A.E. Hughes, T.C. Ang, G.B. Deacon, P. Junk and M. Forsyth, Electrochem and Solid-State Lett., 2007, 10, C72-C75.

40 A. E. Somers, B. R. W. Hinton, C. de Bruin-Dickason, G. B. Deacon, P. C. Junk, and M. Forsyth, *Corr. Sci.,* 2018, **139,** 430-437.

41 C. F. Macrae, I. Sovago, S. J. Cottrell, P. T. A. Galek, P. McCabe, E. Pidcock, M. Platings, G. P. Shields, J. S. Stevens, M. Towler and P. A. Wood, *J. Appl. Crystallogr.*, 2020, **53**, 226–235.

42 CrysAlisPRO v.39. Agilent Technologies Ltd.: Yarnton, Oxfordshire, England.

43 T. M. McPhillips, S. E. McPhillips, H. J. Chiu, A. E. Cohen, A. M. Deacon, P. J. Ellis, E. Garman, A. Gonzalez, N. K. Sauter, R. P. Phizackerley, S. M. Soltis and P. Kuhn, *J. Synchrotron Rad.*, 2002, **9**, 401–406.

44 W. Kabsch, *J. Appl. Crystallogr.*, 1993, 26, 795–800.

45 G. M. Sheldrick, *Acta Crystallogr., Sect. C*, 2015, **71**, 3–8.

46 O. v Dolomanov, L. J. Bourhis, R. J. Gildea, J. A. K. Howard and H. Puschmann, *J. Appl. Crystallogr.,* 2009, **42**, 339–341.

47 American-Standard-Test-Methods in ASTM G31-72, Philadelphia, USA, 2004.

48 N. P. Cowieson, D. Aragao, M. Clift, D. J. Ericsson, C. Gee, S. J. Harrop, N. Mudie, S. Panjikar, J. R. Price, A. Riboldi-Tunnicliffe, R. Williamson and T. Caradoc-Davies, *J. Synchrotron Rad.*, 2015, **22**, 187–190.

GRAPHICAL ABSTRACT:

Synthesis, structure, and corrosion inhibiting properties of RE(III) 3-thiophenecarboxylate complexes

Vidushi Vithana, Zhifang Guo, Glen B. Deacon, Anthony E. Somers and Peter C. Junk

Two series of Rare Earth (RE) 3-thiophencarboxylate (3TPC) complexes have been synthesized by metathesis reactions between a suitable RE salt and Na(3TPC). Based on weight loss measurements and potentiodynamic polarization measurements, the compounds show good corrosion inhibitory properties and act predominantly as anodic inhibitors.